



HAL
open science

Hydrodynamics Characterization of the Impact of Free-Moving Particles in an Air-Lift Membrane Bioreactor

Naila Bouayed, Anthony Cavalier, Christine Lafforgue, Nicolas Dietrich,
Chung-Hak H Lee, Christelle Guigui

► To cite this version:

Naila Bouayed, Anthony Cavalier, Christine Lafforgue, Nicolas Dietrich, Chung-Hak H Lee, et al.. Hydrodynamics Characterization of the Impact of Free-Moving Particles in an Air-Lift Membrane Bioreactor. *Industrial and engineering chemistry research*, 2020, pp.7943-7954. <10.1021/acs.iecr.9b06749>. <hal-02542064>

HAL Id: hal-02542064

<https://insa-toulouse.hal.science/hal-02542064v1>

Submitted on 14 Apr 2020

HAL is a multi-disciplinary open access archive for the deposit and dissemination of scientific research documents, whether they are published or not. The documents may come from teaching and research institutions in France or abroad, or from public or private research centers.

L'archive ouverte pluridisciplinaire **HAL**, est destinée au dépôt et à la diffusion de documents scientifiques de niveau recherche, publiés ou non, émanant des établissements d'enseignement et de recherche français ou étrangers, des laboratoires publics ou privés.



HAL Authorization

1 **HYDRODYNAMICS CHARACTERIZATION OF THE IMPACT OF FREE MOVING**
2 **PARTICLES IN AN AIR-LIFT MEMBRANE BIOREACTOR**

3 N. BOUAYED¹, A. CAVALIER¹, C. LAFFORGUE¹, N. DIETRICH¹, C.H. LEE² & C. GUIGUI^{1,*}

4 1. Toulouse Biotechnology Institute (TBI), Université de Toulouse, CNRS, INRAE, INSA, Toulouse, France

5 2. School of Chemical and Biological Engineering, Seoul National University, Seoul 151-744, Republic of Korea

6 * To whom correspondence should be addressed.

7 Tel.: +33(0)5 61 55 97 90 ; Fax: +33 (0)5 61 55 97 60 ; E-mail: Christelle.Guigui@insa-toulouse.fr

8

9 **Abstract**

10

11 Membrane fouling is one of the most investigated topics in the field of membrane processes
12 because it is the main weakness that prevents membrane bioreactors (MBRs) from being
13 widely applied. With a view to reducing membrane fouling, all the phenomena involved in the
14 operation are worth understanding through a fine-tuned and deep examination. In the present
15 paper, the study focused on the hydrodynamics in an air-lift MBR with a flat sheet membrane,
16 taking into account the application of a specific method for biofouling mitigation adding free
17 moving particles in addition of bubbles injection. The application of this technique creates a
18 complex three-phase gas-liquid-solid contactor in the MBR in terms of hydrodynamics.
19 Therefore, the main objective of this work was to properly characterize, using a Particle
20 Image Velocimetry (PIV) technique, such a system in order to clarify the potential effect of
21 the addition of free moving solid particle on the hydrodynamics and the performances of the
22 MBR. Three different shape of particle have been tested: beads, hollow cylinders and flat
23 sheets. Local hydrodynamic parameters, such as the liquid velocity, the liquid shear stress, or
24 the bubble sizes and velocities were analyzed with and without the presence of solid particles.
25 Specific conclusions are drawn to help future user of this antifouling technique to optimize
26 the design for the solid particle.

27 **Key-words:** Membranes Bioreactors (MBRs), Air-Lift Reactors (ALRs), hydrodynamics,
28 Particle Image Velocimetry, gas-liquid-solid.

29 1. INTRODUCTION

30 Membrane bioreactor (MBR) is the combination of a membrane process like microfiltration
31 or ultrafiltration with a biological wastewater treatment process, the activated sludge process
32 ¹. Over the past two decades, MBRs emerged as a highly potent process in advanced
33 Wastewater Treatment (WWT) owing to their exceptional features. Among all the WWT
34 processes known to date, the innovative MBR technology has been plainly proved to provide
35 excellent effluent quality, total biomass retention, high biomass concentrations, high organic
36 removal efficiency, high organic loading rate and low production of excess sludge. Moreover,
37 the environmental footprint of MBRs has been reported to be low in comparison with
38 conventional processes ^{2,3}. Furthermore, the compactness and the modularity of MBRs design,
39 added to the aforementioned advantages, have promoted their application to treat both
40 industrial and municipal wastewaters (WW) ⁴⁻⁶. Yet, the extensive development of MBRs for
41 WWT is still restricted by some remaining weaknesses among which membrane fouling is the
42 most severe one.

43 Membrane fouling results from the complex combination of several phenomena, such as:
44 deposition and accumulation of solids from the mixed liquor, bacterial growth (also called
45 biofilm), pore clogging, adsorption of secreted products, which lead to the formation of a cake
46 layer onto the membrane surface. Membrane fouling gives rise to an overall reduction in the
47 MBR performance by causing a severe loss of permeability, and thus increase in energy
48 consumption and a heightened need to clean or replace the membrane, which results in a
49 substantial increase in the operating costs. Therefore, in order to mitigate this phenomenon,
50 several cleaning methods have been developed and can be classified into physical, chemical
51 and biological ones.

52 Among the physical methods, one of the most applied ones is air-sparging that consists in the
53 injection of coarse bubbles for the membrane scouring and this method was proved to be

54 efficient to reduce membrane fouling owing to the increased shear stress created by the
55 bubbles on the membrane surface. Moreover, when the air-sparging system was implemented
56 between two flat membranes, an Air-Lift Reactor (ALR) is created, the mitigation of
57 membrane fouling was even more efficient owing to the higher cross flow velocity induced⁷⁻
58 ¹¹.

59 Another method proposed for fouling mitigation belongs to the biological methods and is
60 related to: Quorum Quenching (QQ). QQ consists in the disruption of Quorum Sensing (QS),
61 a cell-to-cell communication mechanism enabling biomass from MBRs to harmonize their
62 behavior for the production of biofilm. Since biofilm is recognized as a major part of the cake
63 layer formed on the membrane surface and responsible of the fouling, QQ was developed as a
64 preventive method for biofouling control in MBRs. The principle of QQ is to degrade, via the
65 addition of an enzyme or an enzyme-producing strain, the signal molecules (AHLs) thanks to
66 which the major part of bacteria in MBRs communicate. Recent works have shown that when
67 QQ bacteria were immobilized into small capsules and implemented in MBRs, the biofouling
68 phenomenon was considerably delayed¹². For more information on the QQ mechanism and
69 its application to MBRs, the reader is invited to consult these reviews^{13,14,1,15}).

70 In the literature, the first media that has been reported is a microbial vessel composed of
71 hollow fibers inside which the QQ bacteria (*Rhodococcus* sp. BH4 or *Pseudomonas* sp. 1A1)
72 are captured (Jahangir et al., 2012; Oh et al., 2012, 2013). The microbial vessel is usually held
73 in a fixed place in the MBR, in opposition to the other Solid media that have been further
74 developed such as QQ beads which are free-moving suspended particles containing the same
75 QQ bacteria. Recently, different shapes such as hollow cylinders or sheets have been
76 developed as Solid media¹⁶⁻¹⁸. In order to study the behavior of these solid media under
77 different operating conditions in the MBR, and their influence on the overall hydrodynamics,
78 the different Solid media were introduced in the lab-scale MBR. In the case of the free-

79 moving Solid media (beads, HC and sheets) the number of suspended objects can be a key
80 parameter, since it is directly correlated with the concentration of QQ bacteria in the MBR. In
81 addition, these objects are also expected to have a mechanical effect on the membrane, thus,
82 the greater their number is, the more pronounced can be the physical washing effect.
83 Fluidization is also a key-phenomenon since it ensures the continuous circulation of Solid
84 media in the reactor and thus, it increases the probability of contact and thereby to exert a
85 mechanical washing effect on the membrane, which was proved to be involved in the
86 biofouling mitigation ¹⁹⁻²³. These findings were in perfect accordance with other studies that
87 widely demonstrated the effective reduction of fouling in MBRs by the addition of solid
88 particles, such as synthetic micro-particles ²⁴, granular activated carbon ²⁵, or other granular
89 scouring agents (reviewed by ²⁶), not only by the sole membrane scouring but also by
90 inducing structural modifications of the microbial flocs and the cake layer ²⁷. Besides, these
91 suspended particles can also play an important role in the hydrodynamics of the reactor which
92 is a key-factor for the overall MBR performance. Therefore, the optimization of the Solid
93 media fluidization is of great interest and was here addressed by taking into account important
94 parameters such as the hydrodynamics (air flowrate), the ALMBR geometry (riser width) and
95 the Solid media (quantity and shape).

96 Hence, the objective of the present work is to study the hydrodynamics of an MBR coupling
97 the two aforementioned techniques: Quorum Quenching particles and Air-Lift Reactor with
98 flat sheet membrane in pure water with inert QQ media. This results in a complex three-phase
99 bioreactor for which the hydrodynamics behavior can be of critical importance to optimize the
100 performance of the system.

2. MATERIAL AND METHODS

The experiments were carried out in a lab-scale MBR with a total working volume of 18 L, composed of an anoxic tank (5 L) and an aerobic tank (13 L), in a similar way to the one described by another research work and to classical industrial configurations (Figure 1) (Li et al., 2015). The MBR was fed in the anoxic tank, which was stirred, and the overflow dropped into the aerobic membrane tank. A PES flat sheet membrane with a total area of 0.1 m² and a pore size of 0.2 μm (Kubota, Japan) was used as a filtration module, and the instantaneous permeate flux was set to 15 L/m² h (LMH). A continuous recirculation from the aerobic tank to the anoxic tank was fixed to 4 L/h. The membrane tank was equipped with an air-sparging system consisting in a coarse air bubbles injection through a perforated tube, composed of two rows of seven 2 mm-holes each, and located at the bottom of membrane (Figure 1).

Two baffles were set on both sides of the membrane, creating an air-lift configuration with three separated parts: an aerated part with an upward circulation called the riser in the center, and two non-aerated parts called the down-comer, on both sides. This air-lift configuration generated an external loop for liquid circulation with no gas recirculation in the down-comer part (figure 1). All the operating conditions are gathered in Table 1.

The MBR was operated in model conditions with tap water with a view to studying the hydrodynamics in the membrane tank, given that the upward movement of bubbles prevails by far over the potential settling of particles in real activated sludge (Brannock et al., 2010, 2009; Yan et al., 2015). All experiments were performed at ambient temperature of 293 K.

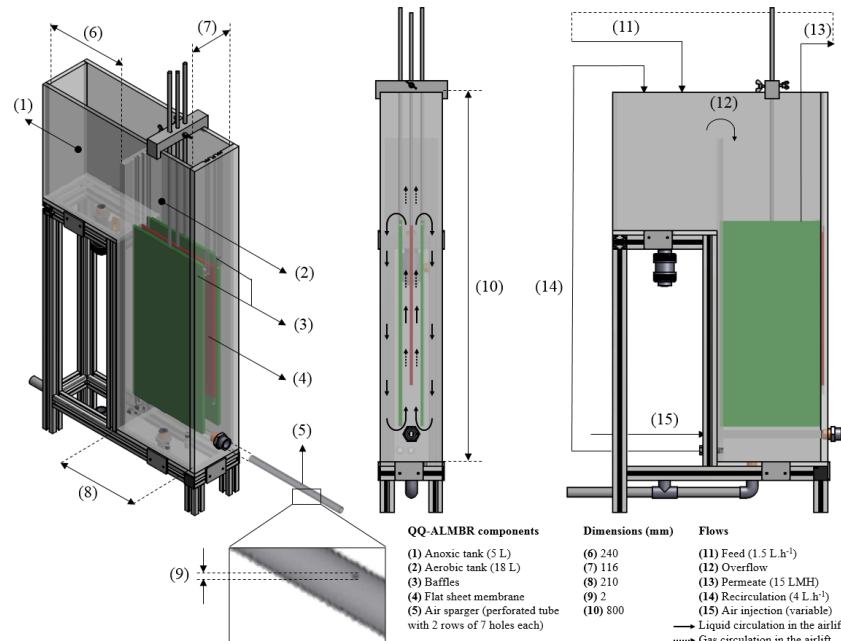


Figure 1 : Diagram of the Quorum Quenching Air-Lift Membrane Bioreactor (QQ-MBR).

123
124

125
126

Table 1 : Air-lift Membrane Bioreactor (MBR) operating conditions.

Operating conditions	
Air-lift	
Riser width $2D_r$ (mm)	[14 ; 30]
Down-comer width $2D_d$ (mm)	[80 ; 64]
Riser cross sectional area A_r (m ²)	[0.00294 ; 0.0063]
Down-comer cross sectional area A_d (m ²)	[0.0168 ; 0.01344]
A_r/A_d ratio (-)	[0.175 ; 0.469]
Liquid height (m)	0.585
Membrane	
Type	Flat sheet
Material	PES
Total area (m ²)	0.1
Average pore size (μm)	~ 0.2
Bioreactor	
Total working volume (L)	18
Total HRT (h)	12
Temperature (°C)	~ 20 (room temperature)
Filtration flux (LMH)	15
SADm (Nm ³ .h ⁻¹ .m ²)	[0.3 ; 0.4 ; 0.75 ; 0.9 ; 1.0]

127

128 In order to study the potential influence of quorum quenching particles implementation on the
 129 MBR from a hydrodynamic point of view, different vacant particle media (with no bacteria
 130 and thus no biological activity) were introduced in the aerobic tank (figure 2). The solid
 131 particles used in this study were made of sodium. The production method consisted in
 132 dripping a homogeneous liquid alginate suspension (complemented without a bacteria
 133 suspension in our case) into a CaCl₂ solution to obtain solid particles, with different shapes, as

134 reported in the literature ^{17,18,20}. The physical properties of the different media are gathered
 135 in Table 2.



136
 137 **Figure 2: Photographs of media used in the study: (a) beads (b) hollow cylinders and (c) sheets.**
 138

139 **Table 2 : Physical characteristics of the Solid media.**

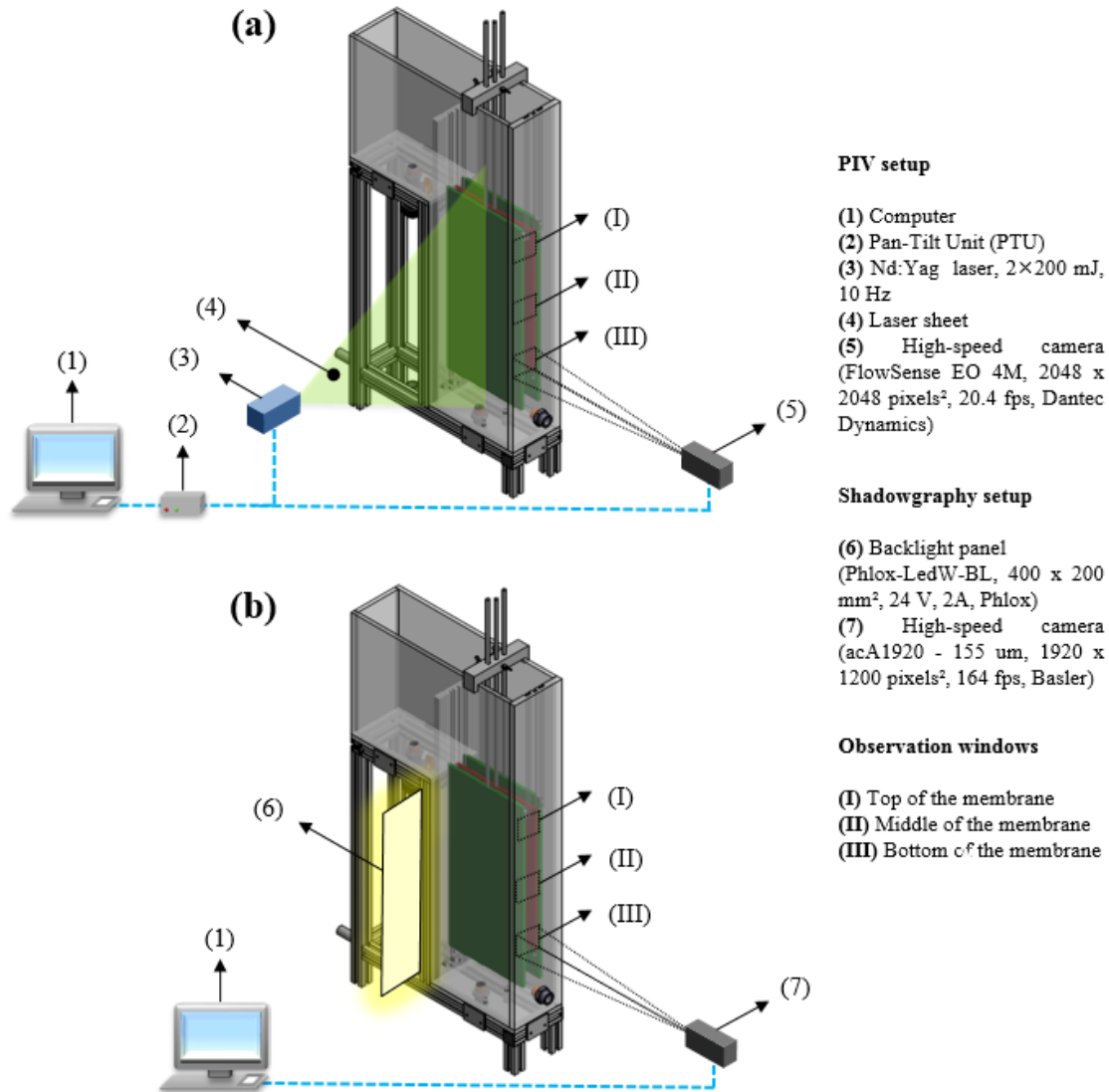
	Beads	Hollow cylinders	Sheets
Dimensions (mm)	Diameter: 3.5	Inner diameter: 1.7 Outer diameter: 3.5 Length: 27	Length: 20 Width: 10 Thickness 0.5
Volume (mm³)	22.5	198.5	100
Surface (mm²)	38.5	455.8	400
Wet density (g.cm⁻³)	1.074 ± 0.002	1.06 ± 0.01	1.063 ± 0.004
Terminal free-falling velocity (m/s)	0.035 ± 0.002	0.024 ± 0.003	0.011 ± 0.002
Total number of introduced media (-)	2600	298	585

140
 141 The hydrodynamics of the MBR was studied by determining velocity fields using the Particle
 142 Image Velocimetry (PIV) technique. In that purpose, the MBR filled with tap water was
 143 seeded with tracer particles (Silver-coated Hollow Glass Spheres (S-HGS), Dantec Dynamics)
 144 with a density of 1.4 g/cm³, a size distribution ranging from 10 to 30 μm and an average
 145 diameter of 15 μm. The middle vertical plane of the reactor was illuminated with a laser sheet
 146 (Nd:YAG unit laser source, DualPower 200-15, class 4, Dantec Dynamics) and the
 147 trajectories of the tracer particles in the liquid flow were captured orthogonally to the laser

148 sheet in different representative areas of about 55 x 55 mm², with a high speed camera
149 (FlowSense EO 4M, 2048 x 2048 pixels², 20.4 fps, Dantec Dynamics) equipped with a 105
150 mm lens (Micro-NIKKOR, 105 mm, Nikon) (figure 3). The acquisition was set to 10 pairs of
151 pictures per second for 25 s to obtain an average flow field in the focused region. The time
152 between two pictures was adjusted according to the velocity induced by the air flowrate and
153 ranged from 0.5 to 5 ms. The images were captured and analyzed using the appropriate
154 software (DynamicStudio 2015a) and the average water velocity fields were obtained by
155 cross-correlating the two consecutive pictures of each pair. Finally, the resulting digitalized
156 data were processed using a Matlab program to determine information about the liquid flow.

157

158 In order to characterize both of the gas phase and the solid phase, a direct visualization
159 technique was used. The experimental setup consisted in a camera (acA1920 - 155 um, 1920
160 x 1200 pixels², 164 fps, Basler) with a 105 mm lens (Micro-NIKKOR, 105 mm, Nikon). A
161 backlight panel (Phlox-LedW-BL, 400 x 200 mm², 24 V, 2A, Phlox) was set up against the
162 back of the aerobic tank in order to illuminate the reactor (figure 3). The acquisition of
163 pictures was set to 200 Hz and lasted 15 s. The images were acquired using the appropriate
164 software (pylon Viewer 64-bit) and then processed using a Matlab program to determine the
165 bubble size and velocity²⁸⁻³¹.



166

167 **Figure 3 : (a) PIV setup and (b) visualization setup for the hydrodynamics characterization.**

168

169 Since the measurements were carried out with optical techniques that needed transparent
 170 media, all the experiments were conducted with tap water and thus without any biological
 171 activity. On the other hand, the PIV requires the addition of tracer particles in a certain
 172 concentration that has to be maintained. For these reasons, the MBR was not fed and the
 173 permeate flux was totally recycled to the anoxic tank to ensure the continuous operation
 174 (figure 1). Also, since both of the recirculation flowrate (4 L/h) and the permeate flux (15
 175 LMH) are relatively low and flow into the anoxic tank (i.e. “far” from the aerobic tank), their
 176 effect on the global hydrodynamic behavior was assumed to be negligible. Therefore, the

177 operating conditions that have been varied were only the ones that can significantly impact
178 the hydrodynamics and the fluidization of the Solid media in the MBR and are explained
179 below.

180 The first important parameter to study was the volume fraction (% v/v) of Solid media to
181 introduce which is defined as the ratio of their total volume to the total liquid volume of the
182 aerobic tank (13 L). Three different volume fractions were selected according to those
183 reported in the literature were used: 0.06 % v/v (Kim et al., 2013), 0.10 % v/v (Maqbool et al.,
184 2015) and 0.45 % v/v (Kim et al., 2015).

185 The distance between the membrane and the baffles, also corresponding to the width of half
186 of the riser part (D_r), could be set to two different positions: 15 mm and 7 mm which is the
187 actual distance separating two membrane panels in industrial flat sheet (FS) modules. This is
188 an important parameter to study because it directly represents the space offered for the solid
189 media and the bubbles to upwardly circulate near the membrane.

190 Another key-parameter to vary was the air flowrate in the air-sparging system. Five different
191 values were chosen based on the literature and ranged from 0.03 to 0.1 Nm³/h (i.e. 0.3 to 1.0
192 in terms of Specific Aeration Demand based on the membrane area (SADm) and 30 to 100
193 Nm³/m³ permeate in terms of Specific Aeration Demand based on the permeate volume
194 (SADp), which fits into the range recommended for MBRs systems (10 to 100 Nm³/m³
195 permeate).

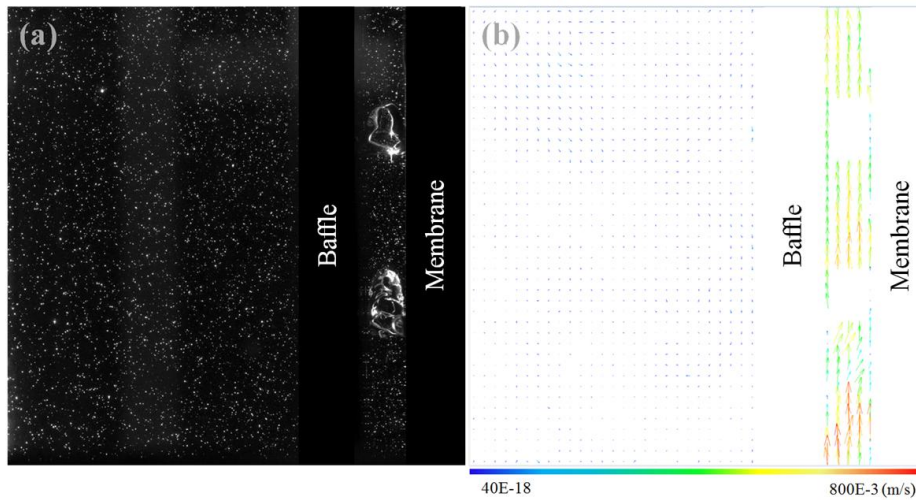
196 Since the camera only allowed the observation of restricted areas (about 55 x 55 mm²), three
197 representative windows (I, II, III) were defined in the top, the middle, and the bottom of the
198 membrane, respectively (figure 2).

199

200 **3. RESULTS AND DISCUSSION**

201 3.1 Hydrodynamics in a two phases flow reactor

202
203 The PIV technique was used to measure velocity fields in the liquid phase^{32,33}. For each
204 operating condition presented, 250 images were recorded, processed, and then digitalized. An
205 example of the obtained raw results by this technique is presented in figure 3 and shows the
206 velocity field in the liquid phase for the observed area. The comparison between the picture
207 (figure 4.a) and the velocity field (figure 4.b) shows that the red areas correspond to the
208 bubbles streaks where higher velocities are induced.



209
210 **Figure 4 : Example of velocity field (b) from the analysis of a PIV image (a) recorded in the MBR**
211 **at the top of the membrane (window I), with $D_r = 7$ mm and under a SADm of $1.0 \text{ Nm}^3 \cdot \text{h}^{-1} \cdot \text{m}^2$.**

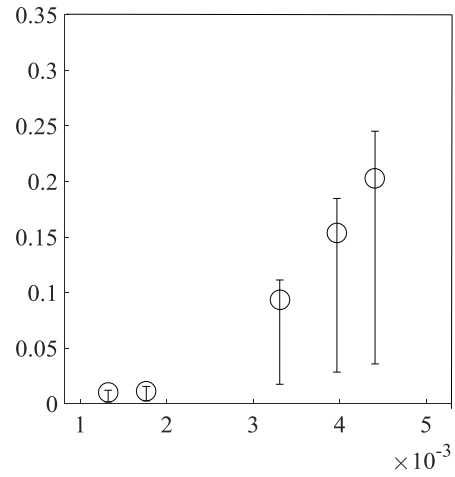
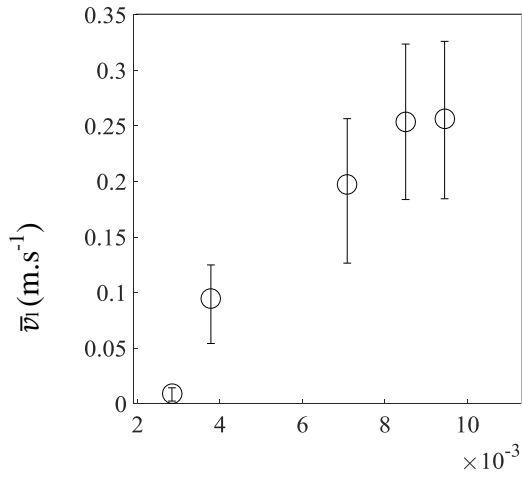
212 In order to focus on the liquid phase, the possible effect of bubbles on images processing was
213 attenuated by averaging the 250 images to get an average velocity field. For each operating
214 condition, the liquid flow was studied in half of the riser part (the MBR is assumed to be
215 symmetrical about the membrane (figure 1)). In this space, the average vertical and horizontal
216 velocities of the liquid were determined and are presented in figure 5 and figure 6,
217 respectively.

218 The error bars represent the standard deviation which indicate the dispersion of data. In that
219 case, the analysis of the error bars shows that the greater the air flowrate is, the wider is the

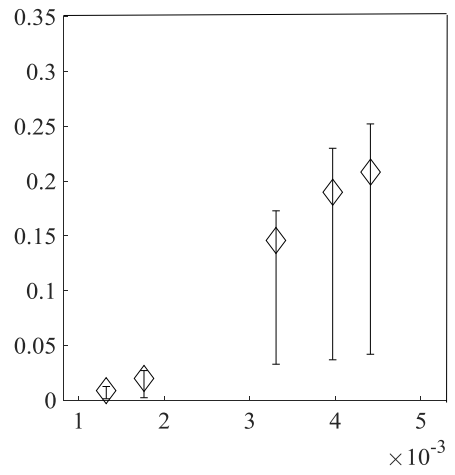
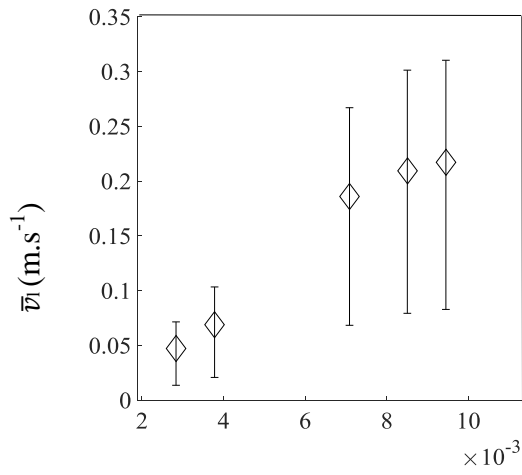
220 range in which the data points spread out. This means that heterogeneous velocity fields tend
221 to be induced at higher air flowrates, with up to $\pm 15\%$ of dispersion from the mean value for
222 the vertical velocity. In the riser part, it appears that the absolute values of the horizontal
223 velocities are more than 1500 times lower than the vertical velocities. This observation
224 confirms that the overall flow in the riser part describes an upward motion that is generated by
225 the rising air bubbles, and that the suction velocity (0.04 mm/s) is too small to induce any
226 horizontal flow near the membrane. Concerning the vertical flow, the average vertical
227 velocity increased with the superficial gas velocity (and thus with air flowrate), and ranged
228 between 0.03 and 0.2 when D_r was set to 7 mm, and between 0.01 and 0.2 when D_r was set to
229 15 mm. These results are in the same order of magnitude as previous studies on MBRs or
230 ALMBRs, that was predictable and consistent according to works reporting the increase of the
231 liquid velocity in ALRs with the superficial gas velocity^{7,8,34,35}. In this study, when D_r was
232 set to 7 mm, it was found that the average liquid velocity in the riser space could be correctly
233 fitted by a power law function ($\bar{V}_l = aU_{gr}^b$) below a certain threshold value of the superficial
234 gas velocity (here, comprised between 0.007 and 0.0085 m.s⁻¹) above which the liquid
235 velocity reaches a plateau value (between 0.15 and 0.25 m.s⁻¹). When D_r was set to 15 mm,
236 all the experimental data were well fitted by a power law function and no plateau value was
237 reached in the investigated range of superficial gas velocity (from 0.0013 to 0.0044 m.s⁻¹).
238 These results are in good agreement with a previous study investigating the hydrodynamics in
239 a rectangular three-phase ALR with suspended polymeric particles in it³⁶.

240

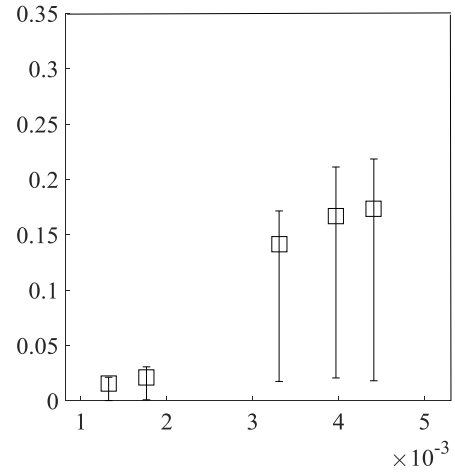
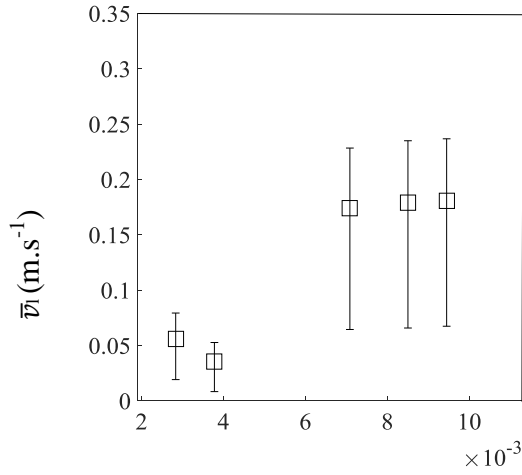
241



242



243



244

245

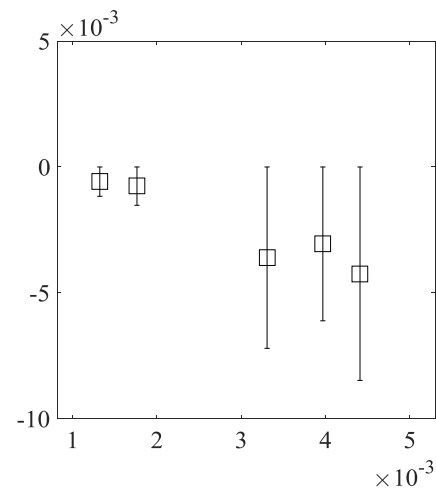
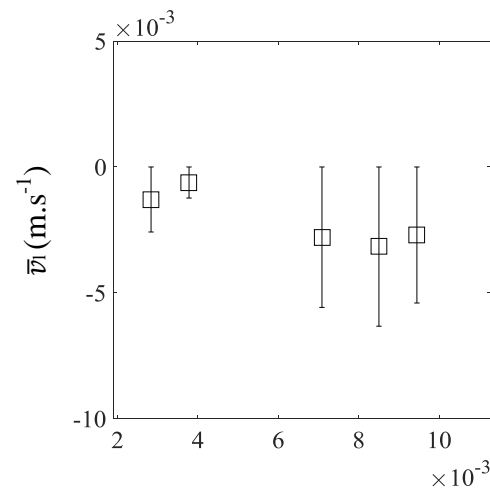
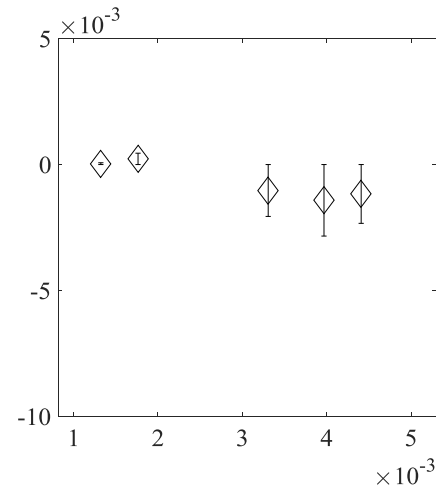
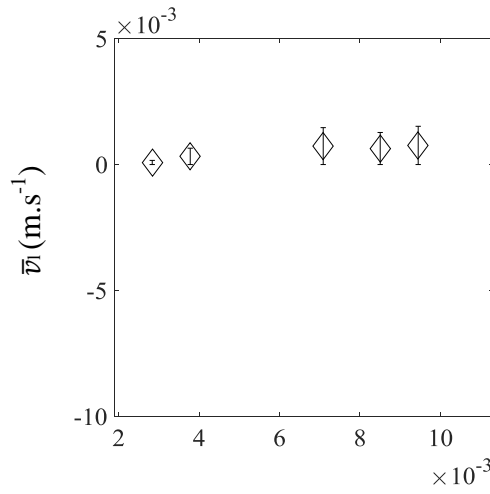
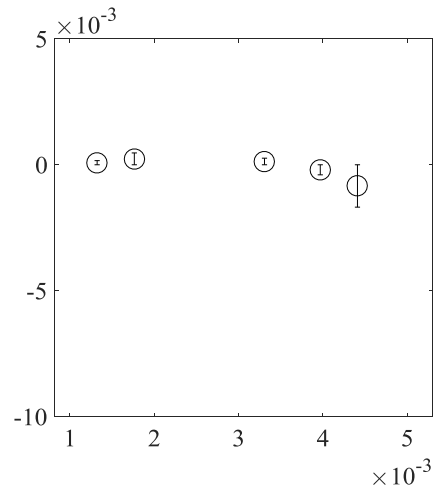
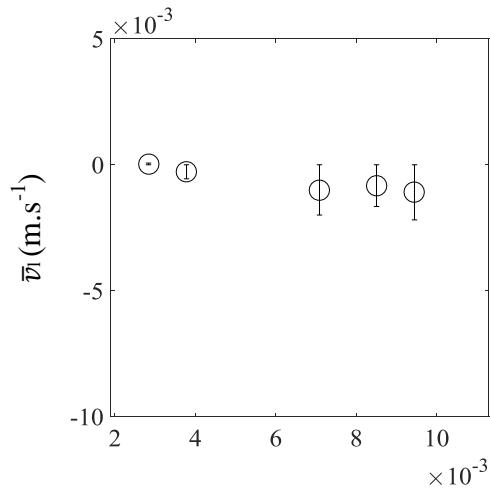
246

247

248

249

Figure 5: Average vertical liquid velocity \bar{v}_l versus superficial gas velocity V_g in the riser at several height: \circ : top; \diamond : middle; \square : bottom. Riser width: Left : 7mm ; right : 15 mm



250

251

252

253

254

255 **Figure 6: Average horizontal liquid velocity \bar{v}_l versus superficial gas velocity V_g in the riser at**

256 **several height: O: top; \diamond : middle; \square : bottom. Riser width: Left : 7mm ; right : 15 mm**

257

258

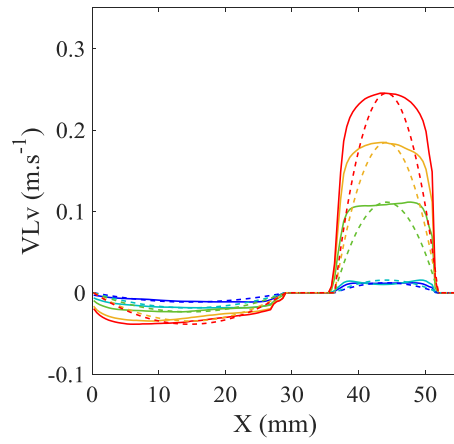
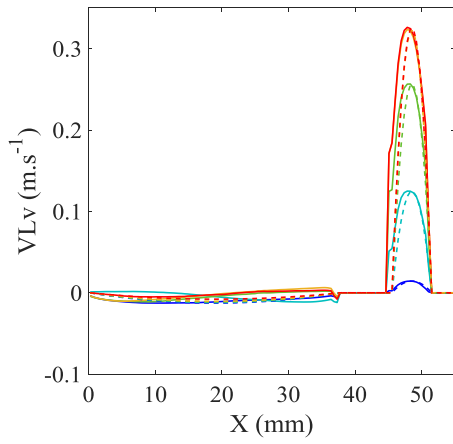
259 The liquid flow regime was characterized by calculating the Reynolds number (Re) based on
 260 the experimental average vertical liquid velocity (\bar{V}_l) in the riser part, according to the
 261 equation n°1, where D_h is the hydraulic diameter (m) (which corresponds in that case to $2D_r$),
 262 ρ is the water density ($\text{kg}\cdot\text{m}^{-3}$) and μ is the water viscosity (Pa.s) at 20°C and 1 atm. The
 263 values of Re ranged between 130 and 3500 when the membrane and the baffle were 7 mm
 264 separated from each other. When this distance was set to 15 mm, the Re numbers ranged from
 265 300 to 5000 for the different air flowrates (table 3).

$$266 \quad Re = \frac{\rho D_h \bar{V}_l}{\mu} \quad (1)$$

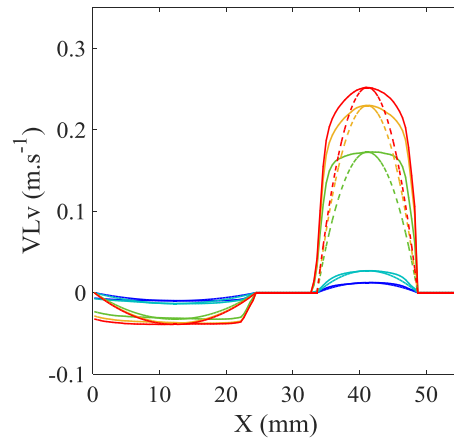
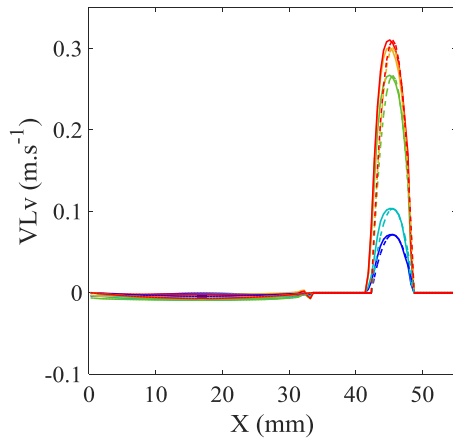
267 The horizontal profile of the experimental local value of the vertical velocity were plotted as
 268 well as the corresponding theoretical profiles, calculated with the average velocity, under the
 269 same conditions (figure 7). The comparison revealed that the experimental velocity profiles
 270 are closer to the theoretical laminar profiles when the riser width (D) is set to 7 mm. On the
 271 other hand, when the riser is 15 mm wide, the velocity profiles are closer to
 272 transitory/turbulent profiles. It is worth keeping in mind that the theoretical equations for
 273 laminar flow only concern the one phase flows, whereas this study deals with a two-phase
 274 flow, which can explain the differences that are still noticeable between the experimental and
 275 theoretical profiles. This observation indicates that the contribution of the gas phase to the
 276 two-phase flow may be less significant in confined spaces (in our case, when the riser is 7 mm
 277 wide).

278
 279 **Table 3: Reynolds number based on the average liquid vertical velocity in the riser part of the MBR.**

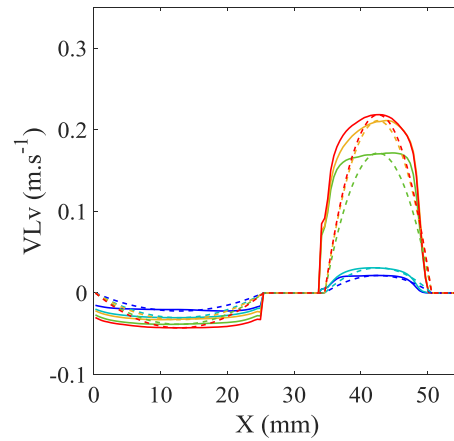
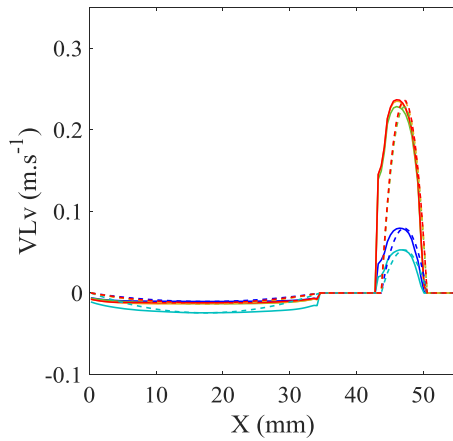
SADm ($\text{Nm}^3\cdot\text{h}^{-1}\cdot\text{m}^2$)	$D_r = 7 \text{ mm}$					$D_r = 15 \text{ mm}$				
	0.3	0.4	0.75	0.9	1	0.3	0.4	0.75	0.9	1
Observation area										
I Top	127	1305	2729	3508	3546	296	332	2767	4553	6007
II Middle	652	954	2569	2895	3002	261	581	4314	5612	6156
III Bottom	777	492	2408	2479	2497	468	635	4197	4944	5140



280

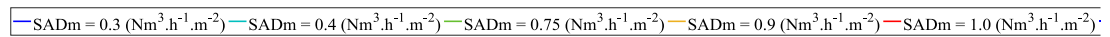


281



282

283



284

Figure 7: Experimental velocity profiles (solid line) and theoretical profiles (dotted line) in the

285

two configurations of MBR (D = 7 mm (left) and D = 15 mm (right)) at several height, under

286

different air flowrates SAD.

287 The membrane shear stress (τ) is defined as the viscosity force induced by the flow on the
288 membrane surface. In the following, the membrane shear stress was obtained from the liquid
289 cross-flow velocity and was calculated at a point of the membrane surface (figure 8),
290 according to the equation n°2, where $V_y(x, y)$ is the vertical liquid velocity measured by the
291 PIV technique at the local considered point (x, y) .

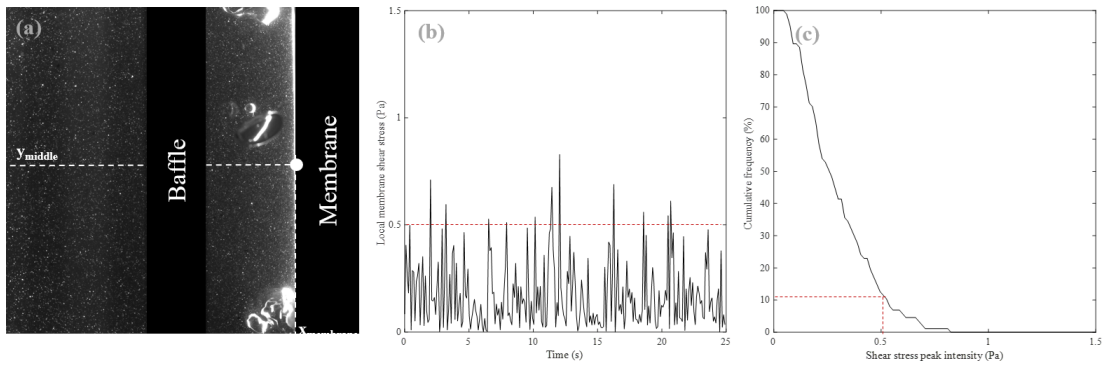
292

$$293 \quad \tau = \mu \left. \frac{\Delta V_y(x,y)}{\Delta x} \right|_{x_{membrane}, y_{middle}} \quad (2)$$

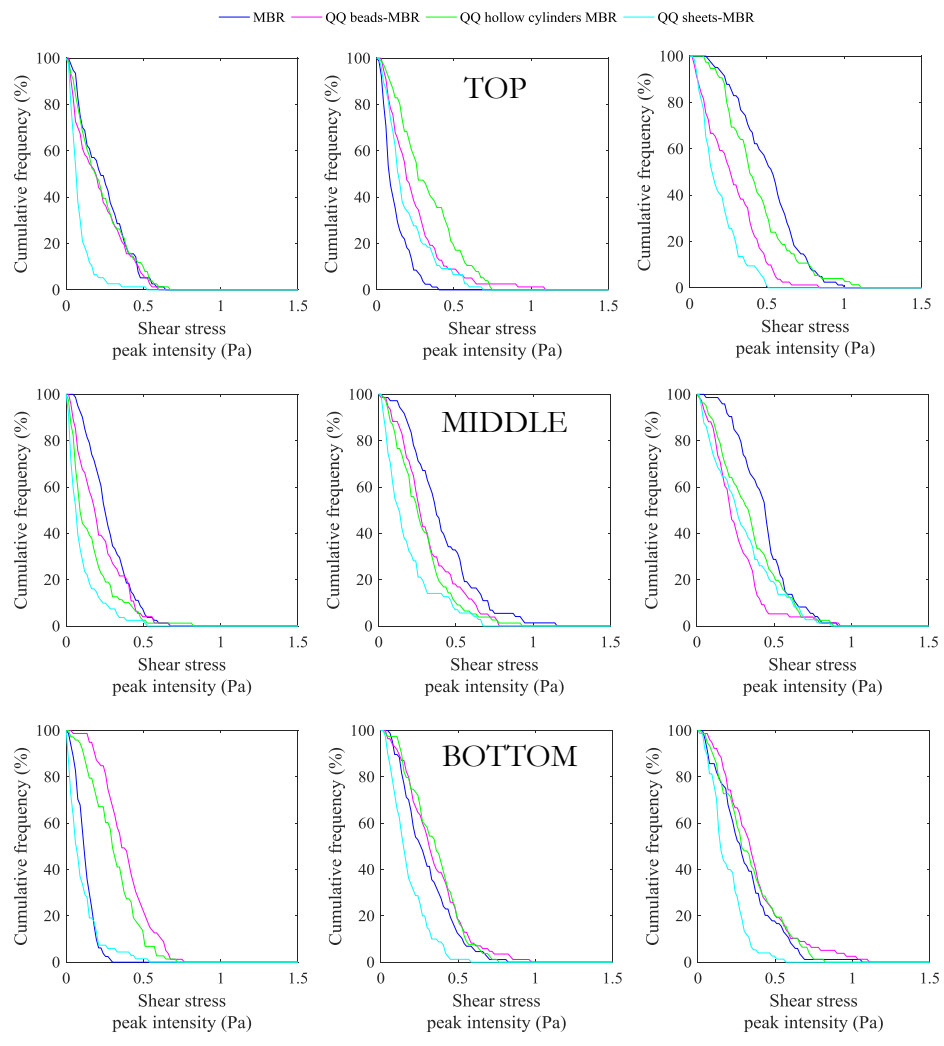
294 The membrane shear stress is highly valuable information when studying aerated MBRs
295 because it is strongly stated that the shear stress created by the bubbles circulation is involved
296 in the biofouling reduction^{8,9}. As a first approach an average membrane shear stress was
297 determined and ranged approximately from 0.005 and 0.2 Pa, which appears lower than the
298 average shear stress previously reported under similar conditions^{10,11}.

299 The local shear stress was determined for each condition and an example of the raw result is
300 presented in figure 8. The profile obtained for the local membrane shear stress is a succession
301 of sharp peaks which are induced by the passage of bubbles of which the streaks create a
302 heightened velocity. The intensity of these peaks appears to be variable, and this may be
303 correlated to the size of bubbles. Therefore it would be assumed that both the shear stress
304 peak number and intensity can be key-factors for biofouling mitigation. Therefore, in order to
305 take into account both of these factors at the same time, a peak size distribution has been
306 determined for each condition. The peak size distribution is presented in terms of cumulative
307 frequency of number of peaks versus the intensity of peaks (figure 8.c). As an example, when
308 the MBR is run with a SADm of $0.9 \text{ Nm}^3 \cdot \text{h} \cdot \text{m}^{-2}$, about 5 % of the shear stress peaks induced
309 have at least an intensity of 0.5 Pa (figure 8.b and 8.c.). When the peak size distribution was
310 comprehensively determined in the MBR under different air flowrates and at the different
311 observation heights, the distribution curves tended to be shifted to the right when the airflow

312 rate increased, which indicates that intense membrane shear peaks are more likely to be
 313 induced at higher air flowrates (figure 9).



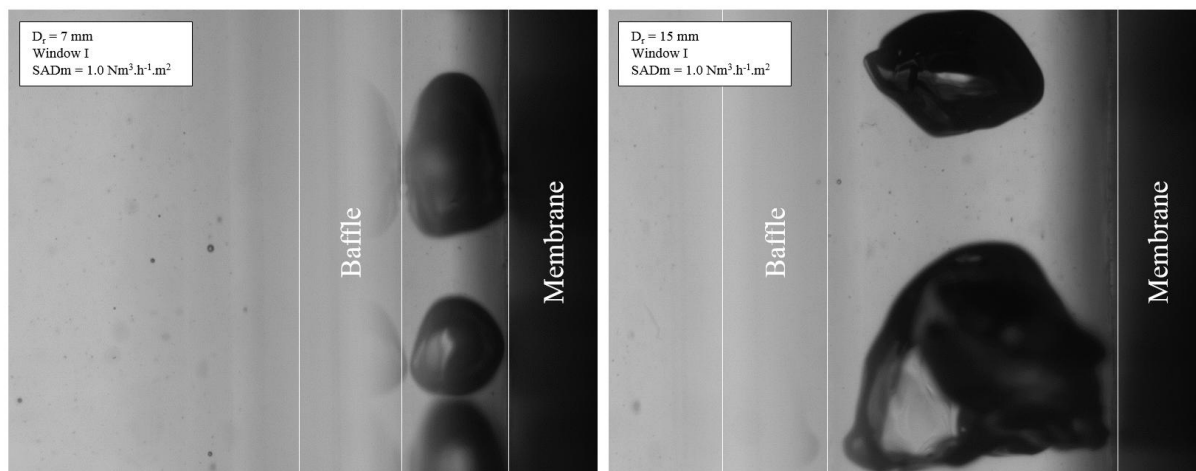
314
 315 **Figure 8 : (a) PIV image, (b) shear stress evolution at the local point ($x_{\text{membrane}}, y_{\text{middle}}$) and (c) its**
 316 **derived shear stress peak distribution, taken at the bottom of the reactor under a SADm of 0.9**
 317 **$\text{Nm}^3 \cdot \text{h}^{-1} \cdot \text{m}^2$ and with $D_r = 15$ mm.**



318
 319 **Figure 9: Local membrane shear stress distribution in the QQ-MBR at 0.45% under different**
 320 **air flowrates (SAD of $0.75 \text{ Nm}^3 \cdot \text{h}^{-1} \cdot \text{m}^2$ (left), $0.9 \text{ Nm}^3 \cdot \text{h}^{-1} \cdot \text{m}^2$ (middle) and $1 \text{ Nm}^3 \cdot \text{h}^{-1} \cdot \text{m}^2$ (right))**
 321 **and in different observation windows.**

322 Therefore, the effect of the air flow rate and the resulting bubble size was analyzed since they
323 could have a great impact on local shear stress. The bubble size was determined by processing
324 images captured with the aforementioned visualization setup (figure 10), to measure the
325 Circle Equivalent Diameter (CED) in terms of surface, under the different operating
326 conditions. For each condition, the images of 10 bubbles were processed and the average
327 bubble size was calculated over these 10 bubbles. The bubble size roughly ranged between
328 4.8 and 7.6 mm when D_r was set to 7 mm wide, and between 4.8 and 9.8 when D_r was 15
329 mm. To our best knowledge, few research studies focused on the characterization of air
330 bubbles in similar geometrical configurations of ALMBRs. Also, the bubble size is strongly
331 dependent on the sparger configuration and the superficial gas velocity. Hence, the
332 comparison with other studies, as well as the validation of the order of magnitude, are in that
333 case hard to achieve. The average bubble size for each condition is plotted versus the
334 superficial gas velocity and presented in figure 11. No clear trend appears when observing the
335 global shape of this plot, which means that the superficial gas velocity seems to have no
336 noticeable influence on the bubble size. However, the comparison of the two columns of
337 plots, reveals that the geometry of the ALMBR has greater influence, since it is possible to
338 notice that the greatest riser width (also corresponding to the greatest ratio of the riser surface
339 to the down-comer surface (A_r/A_d)) gives rise to bigger bubbles (figure 10). This result
340 suggests that the geometrical characteristics of the ALMBR might have an influence on the
341 bubble size, when the superficial gas velocity is kept constant. Concerning the error bars that
342 represent the dispersion of results over the 10 bubbles that were characterized, they are bigger
343 in the case where D_r is set to 15 mm. Thus, it seems that the greatest riser width (and thus the
344 greatest (A_r/A_d) ratio) is most likely to give rise to more heterogeneous population of
345 bubbles in terms of size. Finally, when comparing the results from the different observation
346 windows, it appears that there is no significant modification of the bubbles behavior between

347 the bottom and the top of the ALMBR. It is worth mentioning though that these observations
348 are to be taken carefully because they were deduced from the study of the reduced number of
349 10 bubbles, and a greater number of bubbles should be examined to draw statistically reliable
350 conclusions. Also, the bubble size based on the CED is established on the hypothesis of
351 spherical bubbles which can be far from their real shapes (figure 10). Thus, all these
352 observations concerning the bubble size would need deeper research taking into account a
353 greater number of bubbles as well as a better analysis of their shape.



354

355 **Figure 10: Example of images obtained with the direct visualization method.**

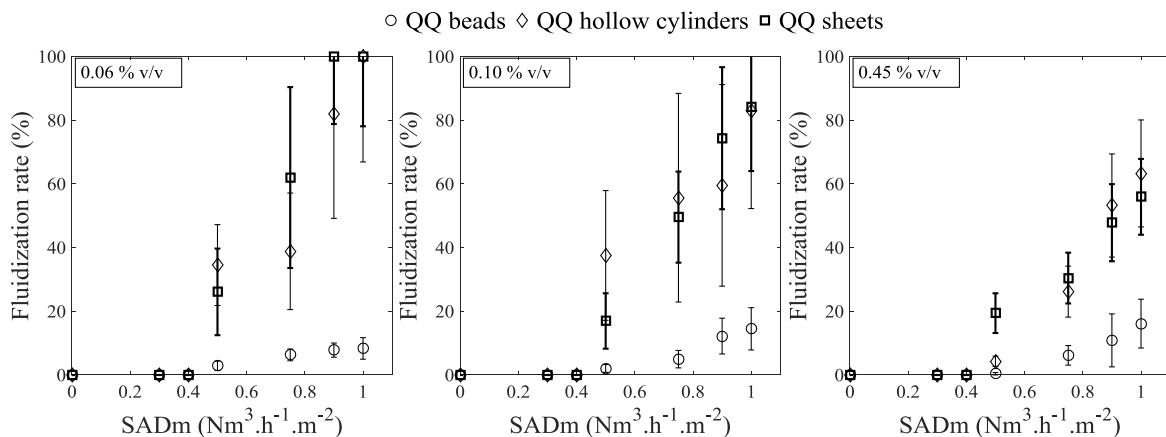
356 However, the average bubble velocity was measured by processing the same images that were
357 previously used for the bubble size determination. The bubble velocity was deduced by
358 tracking the center of each bubble on a series of frames that were acquired at 200 Hz. Thus,
359 the bubble velocity seems to be more reliable information than the bubble size, since no
360 hypothesis is made on the bubble shape. The bubble velocity ranged approximately from 0.4
361 to $0.6 \text{ m}\cdot\text{s}^{-1}$ when the distance between the membrane and the baffle was 7 mm; and from 0.35
362 to $0.65 \text{ m}\cdot\text{s}^{-1}$ when the baffle was 15 mm away from the membrane. This order of magnitude
363 is in accordance with a previous study in which the average bubble velocity was around 0.4
364 $\text{m}\cdot\text{s}^{-1}$ for a population of bubbles among which 66 % had a size comprised between 3 and 5
365 mm. The average bubble velocity is higher than the average liquid velocity in the riser, for the

366 same conditions, which is consistent with the theory since the liquid flow is led by the
367 bubbles rise.

368 3.2 Effect of particle addition

369 Three shape of particles at three concentrations were added in the water. A fluidization rate
370 was defined as the percentage of solid media in suspension in relation to the total number of
371 solid medias initially introduced in the reactor. The fluidization rate was visually measured by
372 counting the suspended media on series of photographs for each experimental condition. A
373 wide range of air flowrates was investigated in order to identify a potential optimal aeration
374 intensity for the media fluidization. The first important result is that no fluidization was
375 observed when D_r was set to 7 mm, probably because the space offered for the media to
376 circulate is too narrow in that configuration. In contrast, when D_r was fixed to 15 mm, the
377 solid media fluidization was observed (figure 11), for the three different shapes when they
378 were introduced at three different volume fractions: 0.06, 0.10 and 0.45 % v/v. The error bars
379 on figure 13 are due to the fact that the fluidization rate was measured on the basis of a
380 relatively limited number of photographs that presented heterogeneous behaviors. Besides, the
381 fluidization of solid media was observed to be a cyclic phenomenon, which means that, after a
382 while, the solid media tend to settle and accumulate in dead zones of the reactor before being
383 dragged again into the flow. It is possible to notice that, for all the shapes and volume
384 fractions, the fluidization rate increases with the aeration, and that there is a critical airflow
385 rate below which the particle tend to settle in the bottom of the reactor which is comprised
386 between 0.4 and 0.5 $\text{Nm}^3 \cdot \text{h}^{-1} \cdot \text{m}^{-2}$ in terms of SADm, (corresponding to 0.0018 and 0.0022 $\text{m} \cdot \text{s}^{-1}$
387 ¹ in terms of superficial gas velocity). Concerning the volume fraction of media introduced,
388 the greater volume fraction (0.45 % v/v) seems to induce lower fluidization rates in
389 comparison to the other volume fractions. This latter observation can be attributed to a density
390 effect referring to the fact that the motion of the solid media in the MBR is no longer

391 completely independent one from another because of their great number. Concerning the
 392 different shapes, the beads appear to reach lower fluidization rates than the hollow cylinders
 393 and sheets. This interesting result can be linked to the physical properties of the hollow
 394 cylinders and sheets, and more specifically to their surface which is more than 10 times
 395 greater than the beads surface (Table 2) and which probably offer them a better behavior in
 396 terms of hydrodynamics and extended lift force. Therefore, it appears that the MBR
 397 configuration of this study is more suitable for the fluidization of hollow cylinders and sheets
 398 than for beads. Thus, the physical washing effect of cylinders and sheets is expected to be
 399 more significant in this kind of ALMBR for the biofouling mitigation, which is in total
 400 accordance with a recent study reporting the enhanced physical washing effect of cylinders at
 401 the same concentration in a lab-scale MBR in comparison to beads (Lee et al., 2016).



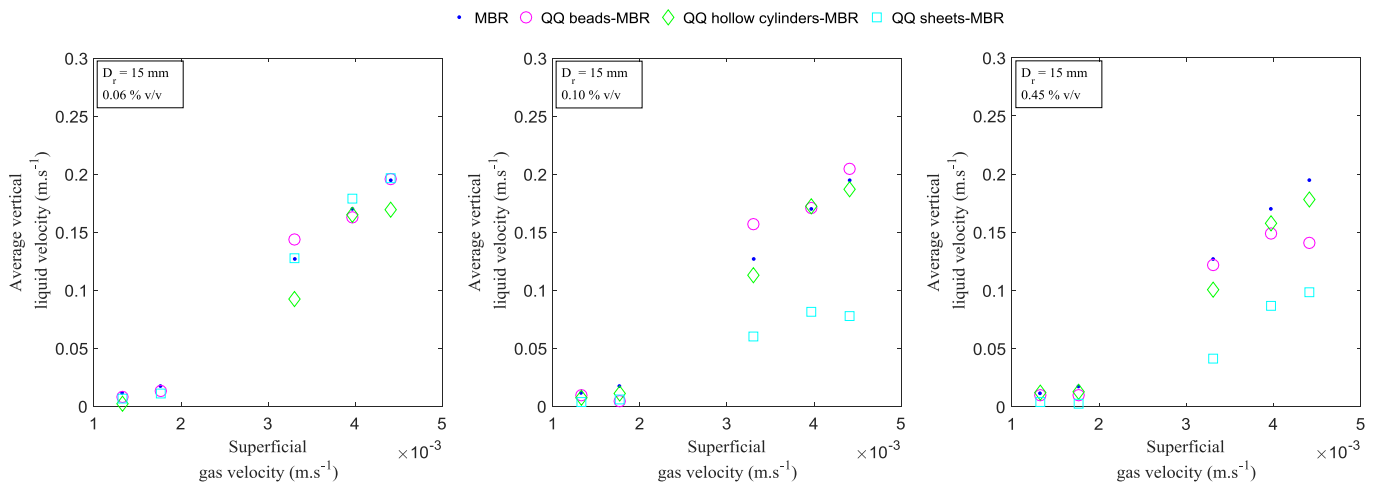
402

403 **Figure 11: Fluidization rate of different shapes of solid media introduced at different volume**
 404 **fraction and measured under different air flowrates.**

405

406 The average liquid velocity in the riser part was measured by the PIV method under different
 407 air flowrates when Solid media were added to the ALMBR at different volume fractions
 408 (0.06, 0.10 and 0.45 %v/v). The results are presented in figure 12. The introduction of solid
 409 media in suspension seems to have no major effect on the global trend followed by the
 410 average liquid velocity in the riser part (compared to figure 5). However, it appears that the

411 increase of the liquid velocity is less pronounced when sheets are added at high volume
 412 fractions (0.1 and 0.45 % v/v). As an example, the average liquid velocity reached with 0.45
 413 % v/v of sheets is around 10 % lower than the liquid velocity in the simple ALMBR with no
 414 media in it, under the same conditions. This observation indicates that the sheets, which were
 415 previously found to have the lowest rising velocity, induce an overall slowdown of the liquid
 416 flow in the riser part, whereas the other shapes of Solid media (beads and hollow cylinders)
 417 have no significant influence on the liquid flow behavior. Similar results were obtained in
 418 previous studies where a slight decrease in the liquid velocity was caused by the introduction
 419 of suspended particles (Couvert et al., 2004).



420
 421 **Figure 12: Evolution of the average horizontal liquid velocity with the superficial gas velocity in**
 422 **the riser part of the ALMBR, for different volume fractions of solid media. $D_r = 15$ mm.**

423 As it was previously done, the Reynolds number was calculated using the average vertical
 424 liquid velocity in the riser when the Solid media were introduced under operating conditions
 425 that enhance their fluidization (volume fraction of 0.45 % v/v, $D_r = 15$ mm and under a high
 426 range of SADm). The results describe similar trend to those of the average liquid velocity,
 427 and again the sheets induce lower values compared to the other Solid media shapes, as well
 428 as, to the sole MBR. These findings indicate that the turbulence phenomena might be
 429 attenuated in presence of sheets.

430 The membrane shear stress in presence of suspended media in the MBR was studied in terms
431 of shear stress peaks distribution for each solid media shape, as it was determined for the
432 MBR alone. The results are gathered in figure 9, for three different air flowrates under which
433 the Solid media fluidize significantly. As it was mentioned previously, the proportions of
434 intense shear stress peaks increased in the MBR when the air flowrate increased. However,
435 this trend is only maintained with the addition of hollow cylinders, whereas the beads and
436 sheets induce random evolution of this same parameter. This observation indicates that,
437 compared to the other shapes, the hollow cylinders might be less likely to impair the proper
438 behavior of the MBR in terms of membrane shear stress created by the liquid flow, which is
439 generated itself by the rising motion of bubbles. In addition, it is possible to notice that the
440 peaks distribution obtained with the addition of solid sheets is almost always below the sole
441 MBR, which indicate that they might reduce the intensity of the shear stress peaks, even
442 though the sheets rise very close to the membrane but with the lowest rising velocity.
443 Nevertheless, the global effect of media on the membrane shear stress is still hard to identify
444 accurately based on this set of results. This probably comes from the difficulty to analyze the
445 membrane shear stress which is deduced from the liquid phase characterization. Besides, the
446 resolution of the PIV technique used for the liquid phase characterization is limited and
447 cannot give information at less than 0.45 μm from the membrane surface, where local
448 phenomena could still occur. The distribution method is a good way to take into account both
449 the number and the intensity of instantaneous shear stress peaks in a local point, but some
450 complementary information is still needed to precisely determine the effect of solid media on
451 this parameter.

452

453 **Conclusion**

454 This work focused on the context of a recent and promising method (Quorum Quenching) for
455 biofouling control in an AL-MBR, from a physical point of view and taking into account the
456 hydrodynamics of such a system. The MBR was first characterized, and the results obtained
457 were globally in good accordance with the literature, in terms of liquid velocity, membrane
458 shear stress and bubbles behavior, which is important, considering the significant advantage
459 of this configuration of reactors at the industrial scale. Secondly, the effect of the addition of
460 solid media on the hydrodynamics was then investigated, firstly by studying their inherent
461 behavior and then, by trying to identify their influence on the ALMBR parameters. The main
462 results of this second part are gathered in table 4 under some specific operating conditions and
463 distinguishing the three phases of the system.

464 - The observation of the solid phase section reveals that the greater is the air flowrate,
465 the better is the fluidization of the solid media. The hollow cylinders seem to fluidize
466 better than the beads, under the same conditions, which can probably be explained by
467 their shape and surface. The velocities of the solid media while rising are in the same
468 order of magnitude, however, the sheets appeared to be slower than the other shapes.
469 Further research is needed though on these parts to know which position and velocity
470 the more advantageous cases for Quorum Quenching would be to correctly mitigate
471 biofouling.

472 - Concerning the liquid phase of the ALMBR, the hollow cylinders and beads induced
473 no noticeable effect on any of the studied parameters, in the operating conditions of
474 this study. However, under these conditions, all the results were in favor of the
475 hypothesis that sheets (the slowest shape of media) seem to induce negative effect on
476 the ALMBR, by slowing down the liquid velocity, reducing the turbulence
477 phenomenon and the membrane shear stress.

478 - In contrast, the effect of media on the gas phase was found to be insignificant in the
 479 conditions of this study.

480 This work not only provides clues about application to MBRs, under a new perspective that
 481 was never approached before: hydrodynamics, but it also actually helps highlighting some
 482 gaps which could be subject to future research. Indeed, knowing that QQ is an efficient
 483 method based on the complex combination of several mechanisms (involving mass transfer,
 484 biochemical/enzymatic reactions, mechanical effect), it could of interest identifying which of
 485 these phenomena are the limiting ones and/or the governing ones.

486 **Table 4: Quantitative properties of Solid media and their qualitative effect on hydrodynamic**
 487 **parameters at a volume fraction of 0.45 % v/v, with $D_r = 15$ mm and under variable air**
 488 **flowrates (SADm). (→ means no effect/↘ means decrease).**

Parameter	beads-MBR	hollow cylinders-MBR	sheets-MBR
Solid phase			
Fluidization rate (%)	0 to 16	0 to 63	0 to 56
Liquid phase			
Average liquid velocity in the riser (m.s ⁻¹)	→	→	↘
Flow regime (turbulence)	→	→	↘
Membrane shear stress	→	→	↘

489

490 **References**

- 491
- 492 (1) Bouayed, N.; Dietrich, N.; Lafforgue, C.; Lee, C.-H.; Guigui, C. Process-Oriented
493 Review of Bacterial Quorum Quenching for Membrane Biofouling Mitigation in
494 Membrane Bioreactors (MBRs). *Membranes* **2016**, *6* (4), 52.
495 <https://doi.org/10.3390/membranes6040052>.
- 496 (2) Gander, M.; Jefferson, B.; Judd, S. Aerobic MBRs for Domestic Wastewater
497 Treatment: A Review with Cost Considerations. *Separation and Purification*
498 *Technology* **2000**, *18* (2), 119–130. [https://doi.org/10.1016/S1383-5866\(99\)00056-8](https://doi.org/10.1016/S1383-5866(99)00056-8).
- 499 (3) Melin, T.; Jefferson, B.; Bixio, D.; Thoeye, C.; De Wilde, W.; De Koning, J.; van der
500 Graaf, J.; Wintgens, T. Membrane Bioreactor Technology for Wastewater Treatment
501 and Reuse. *Desalination* **2006**, *187* (1–3), 271–282.
502 <https://doi.org/10.1016/j.desal.2005.04.086>.
- 503 (4) Brindle, K.; Stephenson, T. The Application of Membrane Biological Reactors for the
504 Treatment of Wastewaters. *Biotechnol. Bioeng.* **1996**, *49* (6), 601–610.
505 [https://doi.org/10.1002/\(SICI\)1097-0290\(19960320\)49:6<601::AID-BIT1>3.0.CO;2-S](https://doi.org/10.1002/(SICI)1097-0290(19960320)49:6<601::AID-BIT1>3.0.CO;2-S).
- 506 (5) Lin, H.; Peng, W.; Zhang, M.; Chen, J.; Hong, H.; Zhang, Y. A Review on Anaerobic
507 Membrane Bioreactors: Applications, Membrane Fouling and Future Perspectives.
508 *Desalination* **2013**, *314*, 169–188. <https://doi.org/10.1016/j.desal.2013.01.019>.
- 509 (6) Meng, F.; Chae, S.-R.; Drews, A.; Kraume, M.; Shin, H.-S.; Yang, F. Recent Advances
510 in Membrane Bioreactors (MBRs): Membrane Fouling and Membrane Material. *Water*
511 *Research* **2009**, *43* (6), 1489–1512. <https://doi.org/10.1016/j.watres.2008.12.044>.
- 512 (7) Liu, R.; Huang, X.; Sun, Y. F.; Qian, Y. Hydrodynamic Effect on Sludge Accumulation
513 over Membrane Surfaces in a Submerged Membrane Bioreactor. *Process Biochemistry*
514 **2003**, *39* (2), 157–163. [https://doi.org/10.1016/S0032-9592\(03\)00022-0](https://doi.org/10.1016/S0032-9592(03)00022-0).
- 515 (8) Liu, R.; Huang, X.; Wang, C.; Chen, L.; Qian, Y. Study on Hydraulic Characteristics in
516 a Submerged Membrane Bioreactor Process. *Process Biochemistry* **2000**, *36* (3), 249–
517 254. [https://doi.org/10.1016/S0032-9592\(00\)00210-7](https://doi.org/10.1016/S0032-9592(00)00210-7).
- 518 (9) Prieske, H.; Drews, A.; Kraume, M. Prediction of the Circulation Velocity in a
519 Membrane Bioreactor. *Desalination* **2008**, *231* (1), 219–226.
520 <https://doi.org/10.1016/j.desal.2007.12.010>.
- 521 (10) Yan, X.; Wu, Q.; Sun, J.; Liang, P.; Zhang, X.; Xiao, K.; Huang, X. Hydrodynamic
522 Optimization of Membrane Bioreactor by Horizontal Geometry Modification Using
523 Computational Fluid Dynamics. *Bioresource Technology* **2016**, *200*, 328–334.
524 <https://doi.org/10.1016/j.biortech.2015.10.050>.
- 525 (11) Yan, X.; Xiao, K.; Liang, S.; Lei, T.; Liang, P.; Xue, T.; Yu, K.; Guan, J.; Huang, X.
526 Hydraulic Optimization of Membrane Bioreactor via Baffle Modification Using
527 Computational Fluid Dynamics. *Bioresource Technology* **2015**, *175*, 633–637.
528 <https://doi.org/10.1016/j.biortech.2014.10.133>.
- 529 (12) Oh, H.-S.; Yeon, K.-M.; Yang, C.-S.; Kim, S.-R.; Lee, C.-H.; Park, S. Y.; Han, J. Y.;
530 Lee, J.-K. Control of Membrane Biofouling in MBR for Wastewater Treatment by
531 Quorum Quenching Bacteria Encapsulated in Microporous Membrane. *Environ. Sci.*
532 *Technol.* **2012**, *46* (9), 4877–4884. <https://doi.org/10.1021/es204312u>.
- 533 (13) Siddiqui, M. F.; Sakinah, M.; Singh, L.; Zularisam, A. W. Targeting N-Acyl-
534 Homoserine-Lactones to Mitigate Membrane Biofouling Based on Quorum Sensing
535 Using a Biofouling Reducer. *Journal of Biotechnology* **2012**, *161* (3), 190–197.
536 <https://doi.org/10.1016/j.jbiotec.2012.06.029>.
- 537 (14) Siddiqui, M. F.; Rzechowicz, M.; Harvey, W.; Zularisam, A. W.; Anthony, G. F.
538 Quorum Sensing Based Membrane Biofouling Control for Water Treatment: A

- 539 Review. *Journal of Water Process Engineering* **2015**, 7, 112–122.
540 <https://doi.org/10.1016/j.jwpe.2015.06.003>.
- 541 (15) Köse-Mutlu, B.; Ergön-Can, T.; Koyuncu, I.; Lee, C.-H.; Köse-Mutlu, B.; Ergön-Can,
542 T.; Koyuncu, I.; Lee, C.-H. Quorum Quenching for Effective Control of Biofouling in
543 Membrane Bioreactor: A Comprehensive Review of Approaches, Applications, and
544 Challenges. *Environmental Engineering Research* **2019**, 24 (4), 543–558.
545 <https://doi.org/10.4491/eer.2018.380>.
- 546 (16) Lee, S.; Lee, S. H.; Lee, K.; Kwon, H.; Nahm, C. H.; Lee, C.-H.; Park, P.-K.; Choo, K.-
547 H.; Lee, J.-K.; Oh, H.-S. Effect of the Shape and Size of Quorum Quenching Media on
548 Biofouling Control in Membrane Bioreactors for Wastewater Treatment. *J. Microbiol.*
549 *Biotechnol.* **2016**. <https://doi.org/10.4014/jmb.1605.05021>.
- 550 (17) Lee, S. H.; Lee, S.; Lee, K.; Nahm, C. H.; Kwon, H.; Oh, H.-S.; Won, Y.-J.; Choo, K.-
551 H.; Lee, C.-H.; Park, P.-K. More Efficient Media Design for Enhanced Biofouling
552 Control in a Membrane Bioreactor: Quorum Quenching Bacteria Entrapping Hollow
553 Cylinder. *Environ. Sci. Technol.* **2016**, 50 (16), 8596–8604.
554 <https://doi.org/10.1021/acs.est.6b01221>.
- 555 (18) Nahm, C. H.; Choi, D.-C.; Kwon, H.; Lee, S.; Lee, S. H.; Lee, K.; Choo, K.-H.; Lee, J.-
556 K.; Lee, C.-H.; Park, P.-K. Application of Quorum Quenching Bacteria Entrapping
557 Sheets to Enhance Biofouling Control in a Membrane Bioreactor with a Hollow Fiber
558 Module. *Journal of Membrane Science* **2017**, 526, 264–271.
559 <https://doi.org/10.1016/j.memsci.2016.12.046>.
- 560 (19) Kim, S.-R.; Lee, K.-B.; Kim, J.-E.; Won, Y.-J.; Yeon, K.-M.; Lee, C.-H.; Lim, D.-J.
561 Macroencapsulation of Quorum Quenching Bacteria by Polymeric Membrane Layer
562 and Its Application to MBR for Biofouling Control. *Journal of Membrane Science*
563 **2015**, 473, 109–117. <https://doi.org/10.1016/j.memsci.2014.09.009>.
- 564 (20) Kim, S.-R.; Oh, H.-S.; Jo, S.-J.; Yeon, K.-M.; Lee, C.-H.; Lim, D.-J.; Lee, C.-H.; Lee,
565 J.-K. Biofouling Control with Bead-Entrapped Quorum Quenching Bacteria in
566 Membrane Bioreactors: Physical and Biological Effects. *Environ. Sci. Technol.* **2013**,
567 47 (2), 836–842. <https://doi.org/10.1021/es303995s>.
- 568 (21) Köse-Mutlu, B.; Ergön-Can, T.; Koyuncu, İ.; Lee, C.-H. Quorum Quenching MBR
569 Operations for Biofouling Control under Different Operation Conditions and Using
570 Different Immobilization Media. *Desalination and Water Treatment* **2015**, 0 (0), 1–11.
571 <https://doi.org/10.1080/19443994.2015.1086899>.
- 572 (22) Lee, S.; Park, S.-K.; Kwon, H.; Lee, S. H.; Lee, K.; Nahm, C. H.; Jo, S. J.; Oh, H.-S.;
573 Park, P.-K.; Choo, K.-H.; et al. Crossing the Border between Laboratory and Field:
574 Bacterial Quorum Quenching for Anti-Biofouling Strategy in an MBR. *Environ. Sci.*
575 *Technol.* **2016**. <https://doi.org/10.1021/acs.est.5b04795>.
- 576 (23) Maqbool, T.; Khan, S. J.; Waheed, H.; Lee, C.-H.; Hashmi, I.; Iqbal, H. Membrane
577 Biofouling Retardation and Improved Sludge Characteristics Using Quorum Quenching
578 Bacteria in Submerged Membrane Bioreactor. *Journal of Membrane Science* **2015**,
579 483, 75–83. <https://doi.org/10.1016/j.memsci.2015.02.011>.
- 580 (24) Teychene, B.; Guigui, C.; Cabassud, C. Engineering of an MBR Supernatant Fouling
581 Layer by Fine Particles Addition: A Possible Way to Control Cake Compressibility.
582 *Water Research* **2011**, 45 (5), 2060–2072. <https://doi.org/10.1016/j.watres.2010.12.018>.
- 583 (25) Wu, B.; Zamani, F.; Lim, W.; Liao, D.; Wang, Y.; Liu, Y.; Chew, J. W.; Fane, A. G.
584 Effect of Mechanical Scouring by Granular Activated Carbon (GAC) on Membrane
585 Fouling Mitigation. *Desalination* **2017**, 403, 80–87.
586 <https://doi.org/10.1016/j.desal.2015.12.003>.
- 587 (26) Aslam, M.; Charfi, A.; Lesage, G.; Heran, M.; Kim, J. Membrane Bioreactors for
588 Wastewater Treatment: A Review of Mechanical Cleaning by Scouring Agents to

- 589 Control Membrane Fouling. *Chemical Engineering Journal* **2017**, *307*, 897–913.
590 <https://doi.org/10.1016/j.cej.2016.08.144>.
- 591 (27) Lesage, N.; Sperandio, M.; Cabassud, C. Study of a Hybrid Process: Adsorption on
592 Activated Carbon/Membrane Bioreactor for the Treatment of an Industrial Wastewater.
593 *Chemical Engineering and Processing: Process Intensification* **2008**, *47* (3), 303–307.
594 <https://doi.org/10.1016/j.cep.2007.01.021>.
- 595 (28) Xu, F.; Jimenez, M.; Dietrich, N.; Hébrard, G. Fast Determination of Gas-Liquid
596 Diffusion Coefficient by an Innovative Double Approach. *Chemical Engineering*
597 *Science* **2017**, *170* (Supplement C), 68–76. <https://doi.org/10.1016/j.ces.2017.02.043>.
- 598 (29) Dietrich, N.; Hebrard, G. Visualisation of Gas-Liquid Mass Transfer around a Rising
599 Bubble in a Quiescent Liquid Using an Oxygen Sensitive Dye. *Heat Mass Transfer*
600 **2018**, 1–9. <https://doi.org/10.1007/s00231-018-2297-3>.
- 601 (30) Xu, F.; Cockx, A.; Hébrard, G.; Dietrich, N. Mass Transfer and Diffusion of a Single
602 Bubble Rising in Polymer Solutions. *Ind. Eng. Chem. Res.* **2018**, *57* (44), 15181–
603 15194. <https://doi.org/10.1021/acs.iecr.8b03617>.
- 604 (31) Xu, F.; Hébrard, G.; Dietrich, N. Comparison of Three Different Techniques for Gas-
605 Liquid Mass Transfer Visualization. *International Journal of Heat and Mass Transfer*
606 **2020**, *150*, 119261. <https://doi.org/10.1016/j.ijheatmasstransfer.2019.119261>.
- 607 (32) Xie, X.; Le Men, C.; Dietrich, N.; Schmitz, P.; Fillaudeau, L. Local Hydrodynamic
608 Investigation by PIV and CFD within a Dynamic Filtration Unit under Laminar Flow.
609 *Separation and Purification Technology* **2017**.
610 <https://doi.org/10.1016/j.seppur.2017.04.009>.
- 611 (33) Xie, X.; Dietrich, N.; Fillaudeau, L.; Le Men, C.; Schmitz, P.; Liné, A. Local
612 Hydrodynamics Investigation within a Dynamic Filtration Unit under Laminar Flow.
613 *Chemical Engineering Research and Design* **2018**, *132*, 954–965.
614 <https://doi.org/10.1016/j.cherd.2018.02.018>.
- 615 (34) Bello, R. A.; Robinson, C. W.; Moo-Young, M. Liquid Circulation and Mixing
616 Characteristics of Airlift Contactors. *Can. J. Chem. Eng.* **1984**, *62* (5), 573–577.
617 <https://doi.org/10.1002/cjce.5450620501>.
- 618 (35) Couvert, A.; Bastoul, D.; Roustan, M.; Line, A.; Chatellier, P. Prediction of Liquid
619 Velocity and Gas Hold-up in Rectangular Air-Lift Reactors of Different Scales.
620 *Chemical Engineering and Processing: Process Intensification* **2001**, *40* (2), 113–119.
621 [https://doi.org/10.1016/S0255-2701\(00\)00130-6](https://doi.org/10.1016/S0255-2701(00)00130-6).
- 622 (36) Couvert, A.; Bastoul, D.; Roustan, M.; Chatellier, P. Hydrodynamic and Mass Transfer
623 Study in a Rectangular Three-Phase Air-Lift Loop Reactor. *Chemical Engineering and*
624 *Processing: Process Intensification* **2004**, *43* (11), 1381–1387.
625 <https://doi.org/10.1016/j.cep.2003.06.001>.
626
627
628
629

Hydrodynamics
characterization of
the Impact of free
moving Particles in an
Air-Lift Membrane
Bioreactor

